Applied Thermal Engineering 162 (2019) 114154

Contents lists available at ScienceDirect

Applied Thermal Engineering

journal homepage: www.elsevier.com/locate/apthermeng

Research Paper

The impact of thermal properties on performance of phase change based energy storage systems

Mohammad Parhizi, Ankur Jain*

Mechanical and Aerospace Engineering Department, University of Texas at Arlington, Arlington, TX, USA

HIGHLIGHTS

- Analyzes performance of phase change energy storage systems.
- Derives expressions for rate of energy stored and energy storage density.
- Determines dependence of performance parameters on thermophysical properties.
- Shows that thermal conductivity enhancement may reduce energy storage density.
- Results expand our understanding of performance of phase change based energy storage systems.

ARTICLE INFO

Keywords:
Thermal energy storage
Phase change energy storage
Analytical modeling
Energy storage density

ABSTRACT

Phase change materials (PCMs) are used commonly for thermal energy storage and thermal management. Typically, a PCM utilizes its large latent heat to absorb and store energy from a source. The rate of energy stored (W) and energy storage density (J/m^3) over a certain time period are both important performance parameters of a phase change based energy storage system. While significant experimental research has been carried out to improve thermal conductivity of PCMs, there is a lack of theoretical understanding of how thermal conductivity and other thermophysical properties affect these performance parameters. This paper presents a theoretical heat transfer model to predict the rate of energy storage and energy storage density as functions of PCM thermal properties. Using perturbation method based techniques, expressions for these parameters are derived for two geometries, first for a simplified assumption of constant temperature at the source-PCM interface, and then for a more realistic scenario of time-dependent interface temperature. Results indicate that while increasing thermal conductivity results in improvement in rate of energy stored, the energy storage density does not change for a Cartesian system and actually decreases for cylindrical system. This shows that using a high thermal conductivity PCM may not be ideal when energy must be stored compactly because while this increases the total energy absorbed, it also results in greater rate of melting, which reduces the energy storage density. Results also provide guidelines for material selection for phase change based energy storage systems. For example, a trade-off in the choice between materials of disparate thermal properties is identified in terms of whether the rate of energy stored or energy storage density is paramount. Differences in the performance of Cartesian and cylindrical systems is investigated. Theoretical results presented in this work highlight various performance trade-offs related to the thermal properties of the PCM and help understand the impact of thermal conductivity enhancement on phase change energy storage performance.

1. Introduction

Solid-liquid phase change occurs in a number of engineering applications such as thermal management, energy storage, etc. The large latent heat of phase change relative to the magnitude of typical sensible heat is utilized commonly for designing effective thermal management [1] or energy storage techniques [2]. In both cases, energy is absorbed from a source of heat into a phase change material (PCM) that undergoes phase change from solid to liquid. As an example, latent heat storage has been widely investigated for storing energy harnessed from renewable sources [3], and forms a critical part of the infrastructure needed to address the intermittent nature of these sources and ultimately make renewable energy feasible. Compared to other competing mechanisms for energy storage, such as sensible heat [4],

* Corresponding author at: 500 W First St, Rm 211, Arlington, TX 76019, USA.
E-mail address: jaina@uta.edu (A. Jain).

https://doi.org/10.1016/j.applthermaleng.2019.114154
Received 14 February 2019; Received in revised form 12 July 2019; Accepted 19 July 2019
Available online 01 August 2019
1359-4311/

thermochemical [5], electrochemical [6], etc., phase change energy storage offers several advantages such as large rates of energy transfer, large energy storage density, etc. [3].

As the phase change process proceeds, thermal impedance offered by the melted liquid slows down the rate of further melting. This self-limiting nature of phase change energy storage has been recognized to be an important limitation of phase change based energy storage [7], and the energy storage system is often designed to counter these effects, for example by providing fins into the PCM to increase surface area [8], or by enhancing PCM thermal conductivity by introducing nano/micro-particles [9].

Typical PCMs can be divided into two categories – organic PCMs which are usually paraffin based, and inorganic PCMs such as salt hydrates that offer large latent heat [10]. Clearly, thermophysical properties such as thermal conductivity (k), heat capacity (C_p) and latent heat (L) of the PCM play a key role in determining the performance of phase change energy storage. While PCMs are typically chosen for their large values of latent heat, these materials also have low thermal conductivity, in the range of 0.1–2.5 W/mK [11]. Significant research has been reported on enhancing thermal conductivity of PCMs. A variety of techniques such as dispersing particles with high thermal conductivity such as graphite and nickel particles[12], adding carbon fibers [13], using expanded graphite and carbon fibers [14], adding high thermal conductivity promoters [7] and using graphite matrix [15] have been used for PCM thermal conductivity enhancement. Graphite matrix insertion has been shown to increase PCM thermal conductivity to up to 17 $Wm^{-1}K^{-1}$ [16]. Multiple microscale mechanisms have been proposed to explain such enhancement, including Brownian motion which enables the particles to move through the fluid, nano-particles clustering and liquid layering around solid particles [17].

The average rate of energy transferred and stored into the PCM over a certain time period is an important performance parameter for both thermal management and energy storage applications. Further, from a systems perspective, the density of energy stored is also an important parameter in order to ensure compactness of energy storage. High energy storage density can be a critical performance parameter when the space available for energy storage is limited and minimizing system weight is important. These considerations often arise in automotive, aerospace and military applications as well as compact consumer electronic devices. While the total energy stored is determined largely by the integral of heat flux at the PCM-source interface over time, the energy storage density additionally involves the volume of PCM melted over the time period.

While most experimental papers have focused on improving thermal conductivity, which clearly improves the rate of heat transfer from the source into the PCM, one must recognize that an increased thermal conductivity also increases the rate of melting. This is expected to increase the total volume of PCM required, and therefore, may negatively impact energy storage density. Unlike extensive past experimental work, a key gap in the literature pertains to the modeling and analysis of such effects. There is a lack in the literature of analytical models that connect these two key performance parameters – total energy stored and energy storage density – with underlying thermal properties of the PCM. Further, such an analytical model may also play a key role in materials selection. For example, given two candidate phase change materials that differ from each other in the values of both k and C_p, an analytical model may help determine which material is expected to have better performance in terms of total energy stored or energy storage density. In some cases, either one of total energy stored and energy storage density may be more critical than the other, and therefore, the choice of the ideal PCM depends on such system-level considerations.

The simplest model for phase change based energy storage is the case of heat transfer from a constant temperature wall into a PCM. This is indeed the well-known Stefan problem [18,19], for which, progression of the melting front is known to be proportional to $\sqrt{\alpha t}$ where α is the thermal diffusivity of the PCM. For this problem, equations are also available for temperature distribution in the melted material, and therefore, the rate of heat transfer into the PCM [18]. However, similar exact models are lacking for more complicated cases, such as in cylindrical coordinates, or for a heat-generating source surrounded by a PCM, for which, analysis using a time-dependent temperature boundary condition is more realistic than a constant temperature one. These limitations in the literature have made it difficult to optimize phase change based energy storage in practical engineering applications that cannot be reasonably modeled by the simplest, constant-temperature Stefan problem, or that are cylindrical or spherical in nature. Phase change heat transfer problems are, in general, non-linear in nature, making such theoretical analysis challenging.

This paper presents analytical modeling of performance parameters for phase change energy storage in a variety of scenarios. Analysis is presented for a PCM absorbing heat from a hot source, although the case of energy transfer between a PCM And a cold body can be similarly analyzed. The key novelty of this work is that the models presented here help understand the impact of thermal properties such as thermal conductivity and heat capacity on the rate of energy storage and energy storage density. Simplified cases such as heat transfer from a constant temperature wall in Cartesian and cylindrical systems are analyzed first. Perturbation method is used to derive expressions for the average rate of energy storage and energy storage density for cases where an analytical solution is not readily available. Theoretical models are extended to account for more realistic scenarios involving time-dependent temperature boundary conditions, which can represent a heat source with internal heat generation next to the PCM. Results indicate that while the rate of energy storage increases with increasing PCM thermal conductivity in a Cartesian phase change system, the energy storage density remains unchanged. Further, in cylindrical system, an increase in thermal conductivity may actually result in a reduction in energy storage density. By developing a theoretical understanding of the effect of PCM thermal properties on the performance of energy storage, this work addresses a key gap in literature. Results derived here help place ongoing experimental research on thermal conductivity enhancement in perspective, and contribute towards the optimization of practical energy storage systems.

2. Theoretical model

This section derives expressions for the two key performance parameters of phase change energy storage – average rate of energy storage and energy storage density – in Cartesian and cylindrical coordinate systems. Section 2.1 analyzes a simplified model that assumes constant wall temperature, whereas Section 2.2 analyzes cases of internal heat generation in the heat source, modeled by an unsteady temperature boundary condition.

2.1. Energy storage from a constant temperature wall

The thermal interaction between the heat source and PCM can, in the most simplified form, be described as heat transfer from a constant temperature wall. The phase change energy storage system could be designed either in Cartesian and cylindrical geometries. In this subsection, expressions for average rate of energy stored and energy storage density are derived for this simplified case.

2.1.1. Cartesian wall

Fig. 1(a) shows a schematic of a Cartesian, one-dimensional phase change energy storage system, where a PCM, initially at its melting temperature T_m absorbs heat from an infinite wall maintained at a constant temperature T_w. Assuming no fluid flow in the newly formed phase due to forced or natural convection, this is the classical Stefan problem, for which well-known solutions are available [18,19]. The phase change front $y(t)$ is given by

$$y(t) = 2\lambda\sqrt{\alpha t} \tag{1}$$

where α is the thermal diffusivity and λ is the root of the transcendental

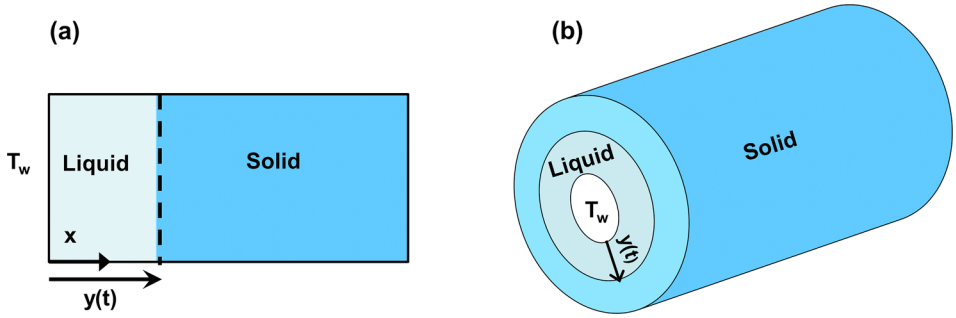

Fig. 1. Schematic of the (a) Cartesian and (b) cylindrical phase change problems consider here.

equation

$$\lambda erf(\lambda) e^{\lambda^2} = \frac{C_p(T_w - T_m)}{L\sqrt{\pi}} \tag{2}$$

Temperature distribution in the newly formed liquid phase is given by [18]

$$T(x, t) = (T_m - T_w)\frac{erf\left(\frac{x}{2\sqrt{\alpha t}}\right)}{\text{erf}(\lambda)} + T_w \tag{3}$$

from where, the average rate of energy absorbed by the PCM up to a given time t can be found to be

$$\dot{Q}_{avg}(t) = \frac{1}{t}\int_0^t -kA\left(\frac{\partial T}{\partial x}\right)_{x=0} d\tau = \frac{-2kA(T_m - T_w)}{\sqrt{\pi\alpha}\, erf(\lambda)\sqrt{t}} \tag{4}$$

Finally, the energy storage density can be found by dividing the total energy absorbed by the volume of PCM melted.

$$Q'''(t) = \frac{\dot{Q}_{avg}(t) \times t}{y(t) \times A} = \rho L e^{\lambda^2} \tag{5}$$

Both $\dot{Q}_{avg}(t)$ and $y(t)$ have the same square root dependence on k, which, therefore, cancels out in the expression of the energy storage density. The final expression of the energy storage density is only a function of density, latent heat and specific heat capacity through λ.

It is assumed in the analysis above that the PCM size can be chosen in advance, based on the knowledge of how much PCM is expected to melt in a given time duration. As a result, the use of $y(t)$ – which is a function of thermal properties – in calculating the volume of PCM melted is appropriate.

Note that in most practical phase change problems, the extent of natural convection is not strong enough to produce significant convective heat transfer due to the relatively small temperature difference and consequently small value of the Rayleigh number. This, together with the considerable complications in the coupled analysis of heat transfer and natural convection justifies neglecting natural convection in the present work.

2.1.2. Cylindrical wall

Consider an infinite bed of PCM absorbing heat from the outer surface of a cylinder of radius R maintained at temperature T_w, as shown in Fig. 1(b). Similar to Section 2.1.1, the PCM is initially at its melting temperature T_m. Unlike the Cartesian Stefan problem discussed in Section 2.1.1, this problem in the cylindrical coordinate system does not have an exact solution. A technique based on perturbation method has been presented for solving this problem, based on an assumption of small Stefan number [20,21].

The governing energy equation in cylindrical coordinate system is given by

$$\frac{1}{r}\frac{\partial}{\partial}\left(r\frac{\partial T}{\partial r}\right) = \frac{1}{\alpha}\frac{\partial T}{\partial t} \tag{6}$$

and the boundary conditions are

$$T = T_w \quad \text{at} r = R \tag{7}$$

$$T = T_m \quad \text{at} r = y(t) \tag{8}$$

$$-k\left(\frac{\partial T}{\partial r}\right)_{r=y(t)} = \rho L\frac{dy}{\partial t} \quad \text{at} r = y(t) \tag{9}$$

Based on perturbation technique discussed in past papers [20,21], t is replaced by phase change front, $y(t)$ in the governing equation and boundary conditions. Temperature distribution is expressed in the form of a series involving powers of the Stefan number, $Ste = \frac{C_p(T_w - T_m)}{L}$. By substituting temperature distribution back in the governing equation and using boundary conditions, similar to the treatment in [20], the phase change front, $y(t)$ is found using an inverse function

$$t = \frac{R^2}{\alpha}\left[\frac{(2(\bar{y}(t))^2\log\bar{y}(t) + 1)}{4} + \frac{Ste}{4\log\bar{y}(t)}((\bar{y}(t))^2\log\bar{y}(t) + \log\bar{y}(t) - (\bar{y}(t))^2 + 1) + \frac{Ste^2}{128(\bar{y}(t))^2\log\bar{y}(t)}(\bar{y}^4(8(\log\bar{y}(t))^3 - 20(\log\bar{y}(t))^2 + 21\log\bar{y}(t) - 8) - 16(\bar{y}(t))^2(\log\bar{y}(t) - 1) - 5\log\bar{y}(t) - 8)\right] \tag{10}$$

where $\bar{y} = \frac{y}{R}$. Note that Eq. (10) corrects a minor error in the final result of similar treatment presented in [20]. Temperature distribution in the newly formed liquid is given by

$$T(r, t) = (\theta_0 + Ste\cdot\theta_1 + Ste^2\cdot\theta_2)(T_w - T_m) + T_m \tag{11}$$

where

$$\theta_0 = 1 - \frac{\log\bar{r}}{\log\bar{y}(t)} \tag{12}$$

$$\theta_1 = \frac{(\bar{r}^2\log\bar{r} - (\bar{y}(t))^2\log\bar{r} - \bar{r}^2 + 1)}{4(\bar{y}(t))^2(\log\bar{y}(t))^3} + \frac{\log\bar{r}((\bar{y}(t))^2 - 1)}{4(\bar{y}(t))^2(\log\bar{y}(t))^4} \tag{13}$$

$$\theta_2 = \frac{1}{64(\bar{y}(t))^4(\log\bar{y}(t))^4}(8\bar{r}^2(\bar{y}(t))^2 - 2\bar{r}^4\log\bar{r} + 10(\bar{y}(t))^4\log\bar{r} - 8\bar{r}^2 + 3\bar{r}^4 - 8(\bar{y}(t))^2 - 8\bar{r}^2 (\bar{y}(t))^2\log\bar{r} + 5) + \frac{1}{128(\bar{y}(t))^4(\log\bar{y}(t))^5}(16\bar{r}^2\log\bar{r} - 40\bar{r}^2(\bar{y}(t))^2 - 10\log\bar{r} - 6\bar{r}^4 \log\bar{r} + 16\bar{r}^2\log\bar{r} - 56(\bar{y}(t))^4\log\bar{r} - 40\bar{r}^2 + 9\bar{r}^4 + 40(\bar{y}(t))^2 + 40\bar{r}^2(\bar{y}(t))^2\log\bar{r} + 31) + \frac{1}{128(\bar{y}(t))^4(\log\bar{y}(t))^6}(((\bar{y}(t))^2 - 1)(31\log\bar{r}) - 40\bar{r}^2\log\bar{r} + 71(\bar{y}(t))^2\log\bar{r} + 40\bar{r}^2 - 40) - \frac{(5\log\bar{r}((\bar{y}(t))^2 - 1)^2)}{16(\bar{y}(t))^4(\log\bar{y}(t))^7} \tag{14}$$

where $\bar{r} = \frac{r}{R}$. As a result, the average rate of energy absorbed by the PCM up to a specific time t can be determined as follows

$$\dot{Q}_{avg}(t) = \frac{1}{t}\int_0^t -k(2\pi Rh)\left(\frac{\partial T}{\partial x}\right)_{r=R} d\tau$$
$$= \frac{1}{t}\int_0^t \Bigg[-k(2\pi Rh)(T_w - T_m)$$
$$\Bigg(\Bigg(\frac{(10(\bar{y}(t))^4 + 8(\bar{y}(t))^2 - 6)}{64(\bar{y}(t))^4(\log\bar{y}(t))^4} - \frac{(5(\bar{y}(t))^2 - 1)^2}{16(\bar{y}(t))^4(\log\bar{y}(t))^7}$$
$$- \frac{(56(\bar{y}(t))^4 + 24(\bar{y}(t))^2 + 44)}{128\bar{y}^4(\log\bar{y}(t))^5} + \frac{((\bar{y}(t))^2 - 1)(71(\bar{y}(t))^2 + 71)}{128(\bar{y}(t))^4(\log\bar{y}(t))^6}\Bigg)Ste^2$$
$$+ \left(\frac{((\bar{y}(t))^2 - 1)}{4(\bar{y}(t))^2(\log\bar{y}(t))^4} - \frac{((\bar{y}(t))^2 + 1)}{4(\bar{y}(t))^2(\log\bar{y}(t))^3}\right)Ste - \frac{1}{\log\bar{y}(t)}\Bigg)\frac{1}{R}\Bigg] d\tau \quad (15)$$

where h is the height of the cylinder. Therefore, the energy storage density can be found by dividing total energy stored in PCM from Eq. (15) by the volume of the melted PCM.

$$Q'''(t) = \frac{\dot{Q}_{avg}(t) \times t}{\pi((y(t))^2 - R^2)h} \quad (16)$$

For any given time t, the phase change front $y(t)$ may be obtained from Eq. (10), following which, Eq. (16) provides the energy storage density.

Note that, in the cylindrical coordinate system, the volume of PCM melted appearing in the denominator of Eq. (16) is a function of y^2 and not y, as was the case in the Cartesian coordinate system. This, along with the complicated expression for Q_{avg} indicates that the lack of dependence of Q''' on k seen for the Cartesian system may not exist for the cylindrical phase change process.

2.2. Energy storage from a heat-generating source: time-dependent temperature boundary condition

The constant wall temperature boundary condition analyzed in Section 2.1, while easily amenable to theoretical analysis, may not accurately model the heat generation process in the source that makes energy available for the phase change material to absorb. For example, internal heat generation in the source may occur due to a chemical reaction, or due to volumetric heat absorption from an external source of radiation. Modeling the heat transfer process within the source makes this a considerably more complicated, coupled heat transfer problem. In order to analyze this system without making it mathematically intractable, the effect of the heat-generating source is modeled with a time-dependent temperature boundary condition at the source-PCM interface. This is a reasonable assumption since the interface temperature is expected to rise with time due to heat generation and thermal conduction within the source. This model is considered in this section for the Cartesian and cylindrical coordinate systems.

2.2.1. Cartesian heat source

This problem is similar to the one analyzed in Section 2.1.1 and shown schematically in Fig. 1(a), where wall temperature is now time-dependent, $T_w(t)$. In this case, the heat transfer problem in the PCM is a Stefan problem with time-dependent temperature boundary condition, for which, a perturbation method based approach is used [20]. Given a time-dependent temperature distribution $T_w(t)$, the heat absorbed as a function of time is given by

$$\dot{Q}_{avg}(t) = \frac{1}{t}\int_0^t -kA\left(\frac{\partial T}{\partial x}\right)_{x=0} d\tau$$
$$= \frac{1}{t}\int_0^\tau -kA(T_m - T_{ref})\Bigg(-\frac{f(t)}{y(t)} - Ste\frac{f(t)\left(f(t) + 2\frac{\dot{f}(t)}{\dot{y}(t)}y(t)\right)}{6y(t)} + \frac{(Ste)^2}{360y(t)}$$
$$\left(f(t)\left(40\left(\frac{\dot{f}(t)}{\dot{y}(t)}\right)^2(\bar{y}(t))^2 + 85f(t)\frac{\dot{f}(t)}{\dot{y}(t)}y(t) + 19f^2(t) + 8\frac{f''(t)}{(\bar{y}(t))^2}f(t)y^2(t)\right)\right)\Bigg) d\tau \quad (17)$$

where

$$f(t) = \frac{T_w(t) - T_m}{T_m - T_{ref}} \quad (18)$$

whereas the phase change propagation front is given by

$$y(t) = \left[2(Ste)\alpha\int_0^t f(\tau)\left(1 - \frac{Ste}{3}f(\tau) + \frac{7Ste^2}{45}f(\tau)^2\right)d\tau\right]^{\frac{1}{2}} \quad (19)$$

Note that expressions for $y(t)$ and $T(x,t)$ are taken from [20]. Further, since the wall temperature is not constant any more, the Stefan number cannot be defined using the wall temperature. Instead, $Ste = \frac{C_p(T_{ref} - T_m)}{L}$, where T_{ref} is a reference temperature. Using Eqs. (17) and (19), the energy storage density is given by

$$Q'''(t) = \frac{\dot{Q}_{avg}(t) \times t}{y(t) \times A} \quad (20)$$

2.2.2. Cylindrical heat source

Fig. 2(b) shows a schematic of a phase change energy storage system in cylindrical coordinate system, in which the wall temperature is now considered to be a function of time $T_w(t)$. Similar to the Cartesian problem, perturbation method is used to solve this time-dependent boundary condition problem. Following the substitution of t with $y(t)$ in the governing equations and separation of terms based on the power of Ste, temperature distribution in the PCM is given by

$$T(r, t) = (\theta_0 + Ste\cdot\theta_1 + Ste^2\cdot\theta_2)(T_w - T_m) - T_m \quad (21)$$

where

$$\theta_0 = -f(t)\left(\frac{\log\bar{r} - \log\bar{y}(t)}{\log\bar{y}(t)}\right) \quad (22)$$

$$\theta_1 = \left(\frac{-f(t)}{4(\bar{y}(t))^2(\log\bar{y}(t))^4}\right)\Bigg(f(t)\log\bar{r} - f(t)\log\bar{y}$$
$$(t) + \frac{\dot{f}(t)\bar{y}(t)(\log\bar{y}(t))^2}{\dot{y}(t)} + \frac{\dot{f}(t)\bar{y}(t)(\log\bar{y}(t))^3}{\dot{y}(t)} + \bar{r}^2 f(t)\log\bar{y}(t) - (\bar{y}(t))^2 f(t)$$
$$\log\bar{r} - \frac{\dot{f}(t)\bar{y}(t)\bar{r}^2(\log\bar{y}(t))^2}{\dot{y}(t)} - \frac{\dot{f}(t)\bar{y}(t)\bar{r}^2(\log\bar{y}(t))^3}{\dot{y}(t)} - \frac{\dot{f}(t)\bar{y}(t)\log\bar{r}(\log\bar{y}(t))^2}{\dot{y}(t)}$$
$$+ \frac{\dot{f}(t)(\bar{y}(t))^3\log\bar{r}\log\bar{y}(t)}{\dot{y}(t)} - f(t)\bar{r}^2\log\bar{r}\log\bar{y}(t) + f(t)\bar{y}^2\log\bar{r}\log\bar{y}$$
$$(t) - \frac{\dot{f}(t)\bar{y}(t)\log\bar{r}\log\bar{y}(t)}{\dot{y}(t)} + \frac{\dot{f}(t)\bar{r}^2\bar{y}(t)\log\bar{r}(\log\bar{y}(t))^2}{\dot{y}(t)}\Bigg) \quad (23)$$

Due to the long and cumbersome nature of the expression for θ_2, it is being included in Appendix 1.

Once the temperature profile is determined, the rate of change of phase change front with time can be found from the boundary condition, Eq. (9) given by

$$\frac{d\bar{y}}{dt} = \frac{(Ste)f(t)}{128(\bar{y}(t))^5(\log\bar{y}(t))^7}(128(\bar{y}(t))^4(\log\bar{y}(t))^6 - 32(Ste)f(t)(\bar{y}(t))^2$$
$$(\log\bar{y}(t))^3(2(\bar{y}(t))^2(\log\bar{y}(t))^2 - 2(\bar{y}(t))^2\log\bar{y} + (\bar{y}(t))^2 - 1)$$
$$+ (Ste)^2(f(t))^2((\bar{y}(t))^4(48(\log\bar{y}(t))^4 - 112(\log\bar{y}(t))^3$$
$$+ 146(\log\bar{y}(t))^2 - 111\log\bar{y}(t) + 40) - 16(\bar{y}(t))^2(2(\log\bar{y}(t))^2$$
$$- 5\log\bar{y}(t)) + 10(\log\bar{y}(t))^2 + 31\log\bar{y}(t) + 40)) \quad (24)$$

Due to the considerable complexity of Eq. (24), analytical integration in order to derive an expression for $y(t)$ similar to Eq. (10) in the case of constant T_w may not be possible. Therefore, phase change front as a function of time is determined in this case by numerical time-stepping based on the time derivative provided by Eq. (24) and using the initial condition of zero melting at $t = 0$. Note that Eq. (24) has a singularity at $t = 0$, which presents a difficulty in initiation of the timestepping approach. In order to address this problem, it is assumed that for a sufficiently small period from $t = 0$ to $t = t^*$, change in the imposed wall temperature $f(t)$ is negligible. This reduces the problem to the cylindrical phase change with constant wall

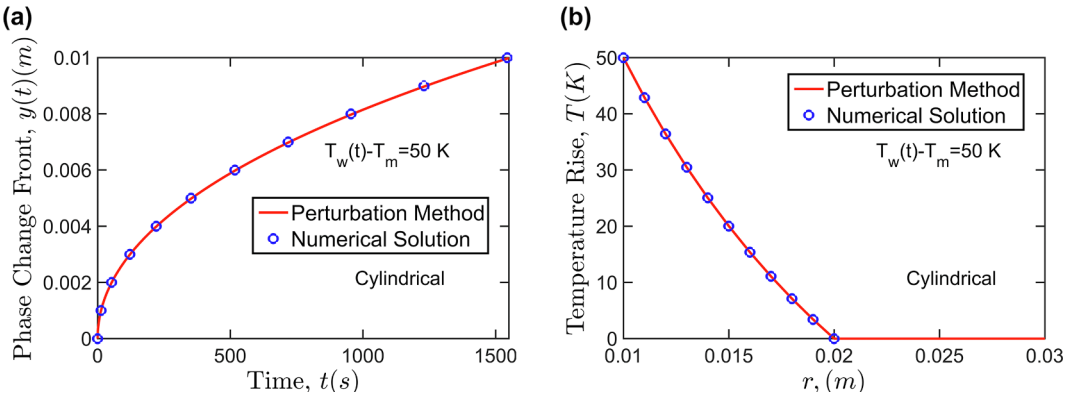

Fig. 2. Comparison of the perturbation method based solutions and a finite element simulation for constant temperature boundary condition: (a) Phase change front, *y(t)* as a function of time for a constant temperature boundary condition $T_w - T_m = 50$ K for the Cartesian problem; (b) Temperature rise as a function of x for the same problem at $t = 1000$ s.

temperature, which has been discussed in Section 2.1.2. Therefore, between $t = 0$ and $t = t^*$, the phase change front is given approximately by Eq. (10). Once *y(t)* is calculated at $t = t^*$, timestepping is carried out for the remaining time period using the derivative provided by Eq. (24). For ensuring minimal impact of this approximation on accuracy, the value of t^* must be chosen to be small. In this work, t^* is chosen to be 0.01% of the total time of interest.

Once *y(t)* has been determined in this manner, the average rate of energy stored can be easily found. Due to its cumbersome nature, the expression for $\dot{Q}_{avg}$ for this case is presented in Appendix 1.

Based on this, the energy storage density can be determined from Eq. (16).

This completes the solution that describes the two key performance parameters of phase change based energy storage in the cylindrical coordinate system for the case of time-dependent temperature boundary condition.

3. Results and discussion

3.1. Model validation

While the constant temperature Cartesian problem discussed in Section 2.1.1 has a well-established solution, validation is desirable for the other solutions discussed in the previous section. This is carried out by comparison with results from a variable time-step finite difference method for phase change problems [18], in which, the space domain is discretized into equal intervals Δx, whereas the time domain is discretized in such a way that during each successive time interval Δt_i, the phase change front *y(t)* propagates by Δx [18]. This results in a set of discretized linear algebraic equations, which are solved using the implicit method.

A phase change material with $k = 0.2\,\mathrm{W m^{-1} K^{-1}}$, $C_p = 2250\,\mathrm{J kg^{-1} K^{-1}}$, $\rho = 810\,\mathrm{kg\,m^{-3}}$ and $L = 270700\,\mathrm{J\,kg^{-1}}$ is considered for comparison between the results derived in Section 2 and the numerical method. Fig. 2(a) shows a comparison of phase change front, *y(t)* as a function of time determined from Eq. (10) and the variable time-step method for the cylindrical coordinate system, with $T_w - T_m = 50\,^{\circ}\mathrm{C}$ and $R = 0.01$ m. The analytical model is found to be in very good agreement with the numerical solution. Fig. 2(b) plots temperature rise as a function of x for the same problem at $t = 1500$ s, showing similarly good agreement between analytical and numerical solutions.

Fig. 3 presents results from similar validation for the analytical models for time-dependent boundary conditions for the two coordinate systems discussed in Section 2.2. Progression of the phase change front is plotted in Fig. 3(a) and (b) for Cartesian and cylindrical systems, respectively. In each case, wall temperature is assumed to vary as $T_w(t) - T_m = 50 + 0.03t$. Good agreement between the two is observed, similar to the results for constant temperature boundary conditions. Figs. 2 and 3 provide validation of the theoretical models for phase change processes discussed in Section 2.

3.2. Effect of k on PCM performance parameters

The effect of thermal conductivity, k on total energy absorbed by the PCM and energy storage density in a Cartesian body is investigated first. Fig. 4(a) and (b) present plots of the average rate of energy stored up to $t = 1000$ s as a function of thermal conductivity for Cartesian and cylindrical bodies, respectively. $T_w - T_m = 50\,^{\circ}\mathrm{C}$ in each case and $R = 0.01$ m for the cylindrical system. Similar plots for the energy storage density at $t = 1000$ s are presented in Fig. 5(a) and (b). Fig. 4 shows that the total rate of energy storage increases with increasing k for both geometries. For the Cartesian system, this originates from the $\sqrt{k}$ dependence of $\dot{Q}_{avg}$, as shown in Eq. (10). Expressions for the cylindrical system, Eq. (15), while more complicated, also show that $\dot{Q}_{avg}$ increases with k. Physically, this occurs because greater k results in greater heat diffusion into the PCM. and consequently greater rate of energy stored in the system. As shown in Fig. 4, this effect is much stronger in Cartesian bodies due to the larger surface area from which heat can be absorbed by the PCM. As shown in Fig. 6, the energy storage density remains constant with increasing k for the Cartesian system, and actually reduces for cylindrical system. This occurs because while increasing PCM thermal conductivity results in greater energy absorbed, it also increases the melted PCM volume. For the Cartesian problem, both $\dot{Q}_{avg}$ and y exhibit a $\sqrt{k}$ dependence, and therefore, these effects exactly cancel each other when determining the energy storage density Q'''. On the other hand, for the cylindrical problem, the effect of increased melting rate dominates over the effect of increased rate of energy stored, thereby resulting in a reduction in energy storage density with increasing thermal conductivity. This shows that while increasing thermal conductivity of PCM improves a key performance parameter – rate of energy absorbed –the other key performance parameter, energy storage density remains the same for the Cartesian system and actually decreases for a cylindrical energy storage system.

This trade-off between the rate of energy stored and energy storage density highlighted by Figs. 4 and 5 is important to recognize because the relative importance of these two performance parameters differs from one application to the other. In applications where it is important to absorb a large amount of energy very rapidly without regard to storage density, increasing k is clearly helpful, regardless of whether the energy storage system is Cartesian or cylindrical. However, when energy storage density is important, for example when energy must be stored compactly, increasing k is not likely to be effective, and in fact, may adversely affect energy storage density for cylindrical energy storage. This happens because in the Cartesian system, the volume of PCM melted has a $\sqrt{k}$ dependence due to linear scaling with *y(t)*, as shown in Eq. (1), whereas in cylindrical system, the dependence is much stronger due to the quadratic dependence of volume of PCM melted on *y(t)* respectively. Thus, for a Cartesian body, thermal conductivity can be increased in order to increase

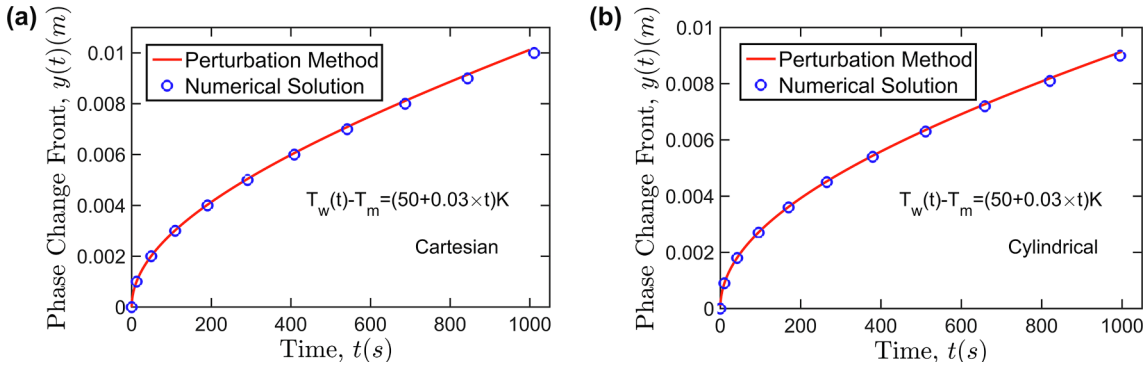

Fig. 3. Comparison of the perturbation method based solutions and a finite element simulation for time-varying temperature boundary condition: (a) Phase change front, *y(t)* as a function of time for a time-dependent temperature boundary condition $T_w(t) - T_m = 50 + 0.03t$ for the Cartesian problem; (b) Phase change front, *y(t)* as a function of time for a constant temperature boundary condition $T_w(t) - T_m = 50 + 0.03t$ for the cylindrical problem.

the rate of heat absorbed without negatively impacting the energy storage density. However, in cylindrical body, such an approach will result in reduced energy storage density. In such a case, optimal system design using the approach presented here may be critical.

For a more comprehensive analysis of how thermal properties affect energy storage performance, colormaps of $\dot{Q}_{avg}$ and Q''' are plotted in Fig. 6 for $T_w - T_m = 50\,^{\circ}\mathrm{C}$ and $t = 1000\,\mathrm{s}$ for a Cartesian system. Latent heat of the PCM is assumed to be $L = 270700\,\mathrm{J\,kg^{-1}}$. Fig. 6(a) shows much stronger dependence of $\dot{Q}_{avg}$ on k than on C_p, indicating that small changes in k are more likely to affect $\dot{Q}_{avg}$ than changes of similar relative magnitude in C_p. However, the impact of these thermal properties on Q''' is quite different, as shown in Fig. 6(b). Q''' remains invariant with changes in k, whereas it increases with increasing C_p. Fig. 6 can be used for performance comparison between different candidate PCMs. For example, three candidate PCMs *A*, *B* and *C* are marked on the colorplots in Fig. 6(a) and (b) in terms of their thermal properties. PCM *A* has higher k but lower C_p than PCM *B*. PCM *C* lies somewhat in the middle of *A* and *B* in terms of both k and C_p. The colorplots in Fig. 6(a) and (b) show that while *A* is expected to have greater rate of energy stored, its performance in terms of energy storage density is poorer than that of *B*. Further, comparing *A* and *C*, it is seen that due to curvature in the color contours in Fig. 6(a), *A* and *C* are expected to result in the same rate of energy stored, while, based on Fig. 6(b), *C* is expected to store this energy much more compactly than *A*. The superior performance of *C* is despite its lower thermal conductivity than *A*, and shows that in some conditions, a material may be an attractive PCM despite relatively lower thermal conductivity.

Similar colorplots of $\dot{Q}_{avg}$ and Q''' for a cylindrical energy storage system are presented in Fig. 7(a) and (b) respectively. Similar to the Cartesian case, it is seen that the rate of energy stored increases with k. However, the energy storage density actually reduces with increasing k. This has several interesting consequences in the choice of thermal properties of candidate PCMs. For example, three candidate PCMs *D*, *E* and *F* are shown in Fig. 7(a) and (b). It is seen that while *D* has greater rate of energy stored compared to *E* due to greater thermal conductivity, its energy storage density is actually lower. On the other hand, *F*, which has the same k as *D* but greater heat capacity, resulting in a high rate of energy stored as well as a high energy storage density.

These examples illustrate the importance of colorplots such as Figs. 6 and 7 in understanding the trade-offs between thermal conductivity and heat capacity in terms of the performance parameters, and in choosing the correct PCM. In general, this choice depends on whether the rate of energy stored or the energy storage density is more critical, as well as on whether the energy storage system is in Cartesian or cylindrical geometry. Results from this section enable quantification of this trade-off, and help choose the best material corresponding to system-level objectives.

3.3. Results with time-dependent boundary conditions

The key results discussed in Section 3.2 pertain to a constant wall temperature boundary condition. However, for practical scenarios where the hot source generates heat at a certain rate, the temperature at the wall may not be constant and may increase over time. This is also true for scenarios where time-varying heat flux impinges on the wall. In such cases, variation in the wall temperature with time must be accounted for using models presented in Section 2.2. This section discusses results on this practical scenario. A linearly increasing wall temperature $T_w(t) - T_m = 50 + 0.03t$ is assumed. Fig. 8(a) and (b) plot the average rate of energy stored as a function of k for Cartesian and cylindrical energy storage systems respectively. Similar plots for energy storage density are presented in Fig. 9(a) and (b). For both Cartesian and cylindrical cases, the rate of energy stored increases with k, similar to the results for constant wall temperature case discussed in the previous section. The energy storage density remains invariant with k in the Cartesian case, whereas it actually reduces with k for the cylindrical case. This is also similar to the

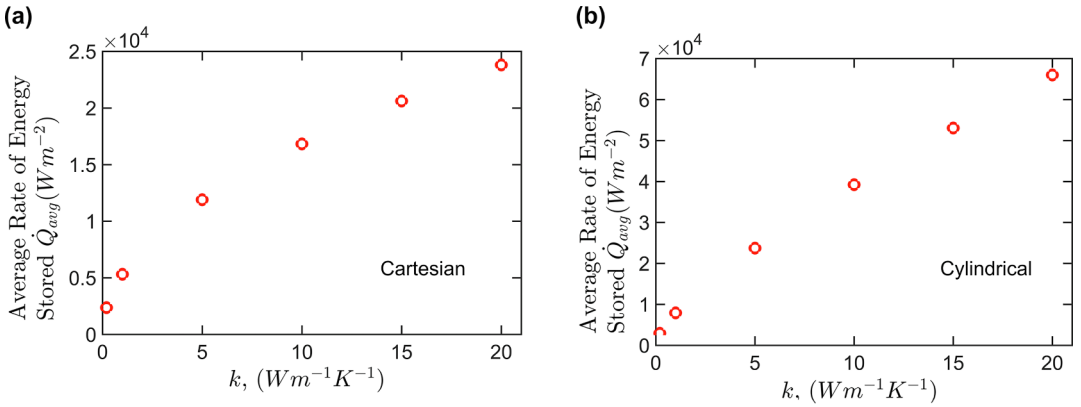

Fig. 4. Effect of thermal conductivity, k on average rate of energy stored per unit area of the source-PCM interface in (a) Cartesian and (b) cylindricalsystemsfor a constant temperature boundary condition $T_w - T_m = 50\,\mathrm{K}$ over a 1000 s time period.

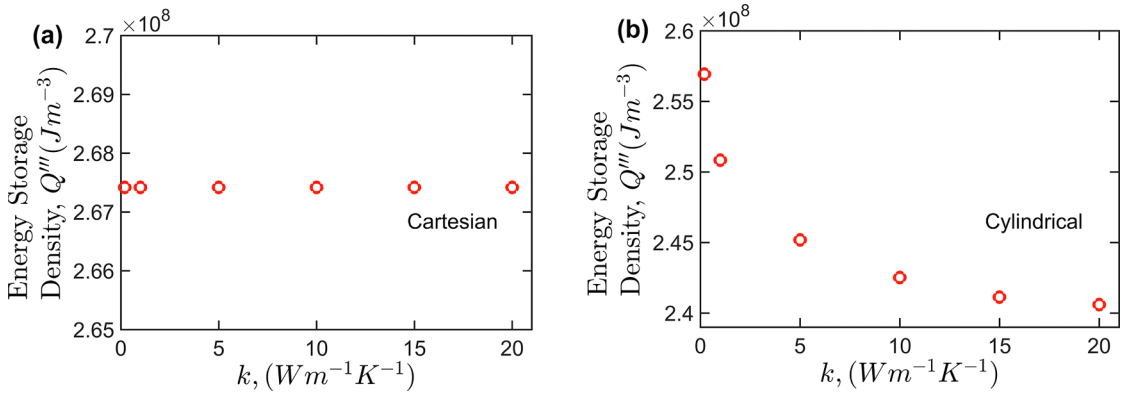

Fig. 5. Effect of thermal conductivity, k on energy storage density in (a) Cartesian and (b) cylindricalsystems for a constant temperature boundary condition $T_w - T_m = 50$ K over a 1000 s time period.

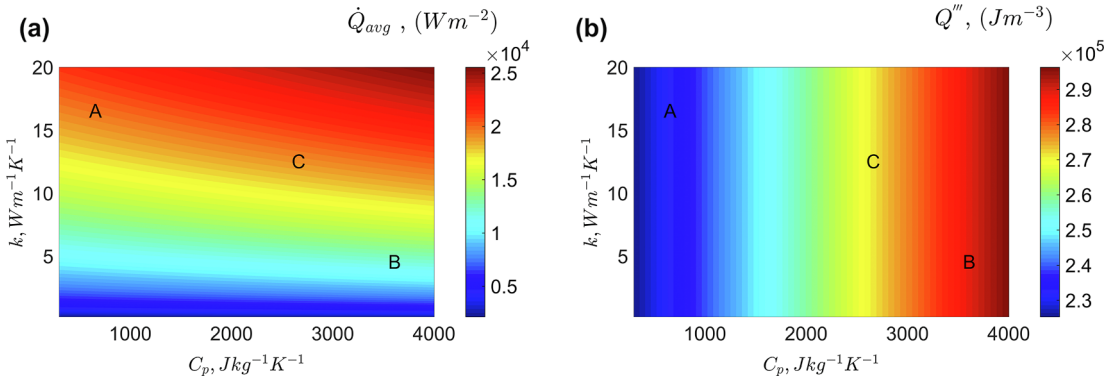

Fig. 6. Colorplots of (a) average rate of energy absorbed by the PCM and (b) energy storage density as function of thermal conductivity and heat capacity in a Cartesian system.

constant wall temperature case. Both $\dot{Q}_{avg}$ and $y(t)$ for the Cartesian case, shown in Eqs. (17) and (19) respectively continue to have a $\sqrt{k}$ dependence, resulting in Q''' remaining independent of k, just like the constant T_w case. These relationships for cylindrical case are more difficult to interpret due to the complexity of the equations.

These plots show that the key results discussed for the constant wall temperature case also hold for the more realistic, time-varying wall temperature case. The method presented here is valid for quantifying the effect of improving PCM thermal conductivity on critical performance parameters in practical engineering applications.

In order to further understand the nature of energy storage performance parameters in case of time-dependent boundary conditions, Fig. 10(a) and (b) plot rate of energy stored and energy storage density as functions of k. Plots are presented for both Cartesian and cylindrical energy storage systems for different expressions for $T_w(t)$. Specifically, linearly increasing wall temperature with different values of slopes $T_w(t) - T_m = A + Bt$ is assumed where A = 50 K and B = 0.01, 0.03, 0.05, 0.07 and 0.09 Ks^{-1}. A time period up to while $t = 1000$ s is considered. Fig. 10(a) indicates that in both Cartesian and cylindrical coordinates, the rate of energy absorbed increases with k, which is consistent with results obtained from Fig. 8. Further, the greater the value of slope B, the larger is the rate of energy absorbed, which is along expected lines due to greater temperature gradient between the wall and PCM. Fig. 10(b) shows that in the Cartesian system, energy storage density is not a function of k, similar to previous results, and also increases with increasing value of B. Increasing the value of B affects increases the rate of heat absorbed as well as the phase change front propagation. The impact on the former is weaker, due to which,

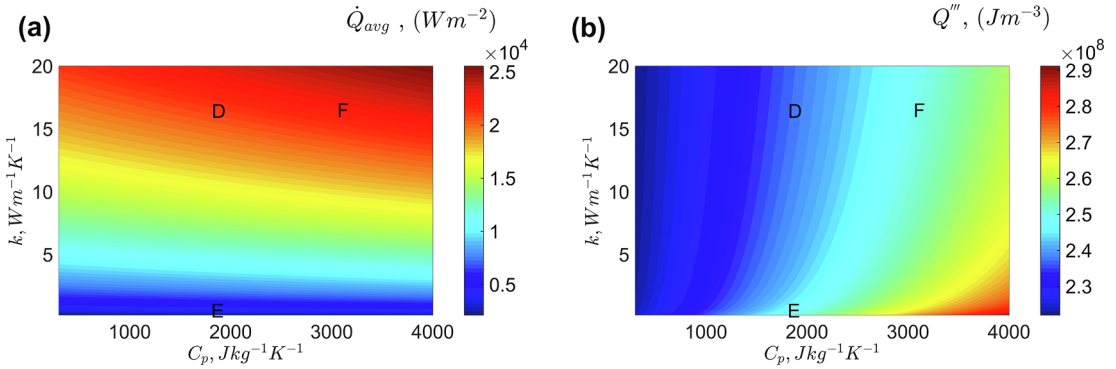

Fig. 7. Colorplots of (a) average rate of energy absorbed by the PCM and (b) energy storage density as function of thermal conductivity and heat capacity in a cylindrical system.

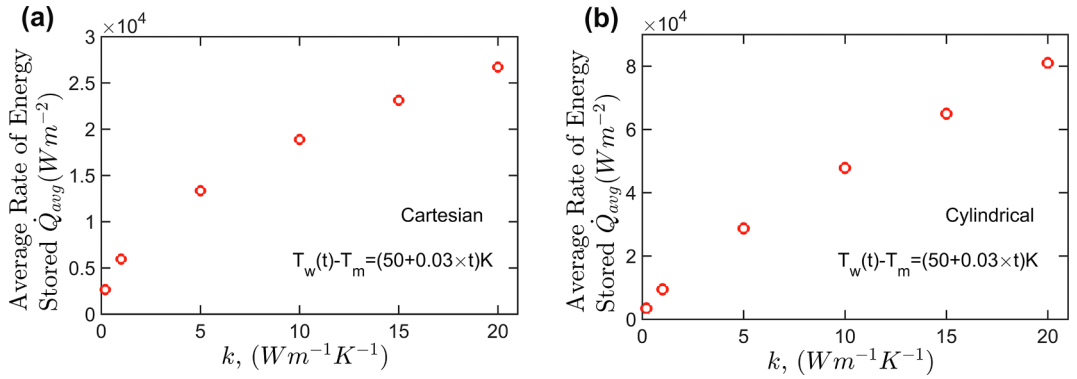

Fig. 8. Effect of thermal conductivity, k on average rate of energy stored per unit area of the source-PCM interface in (a) Cartesian and (b) cylindrical coordinate systems for a time-dependent temperature boundary condition $T_w(t) - T_m = 50 + 0.03t$ over a 1000 s time period.

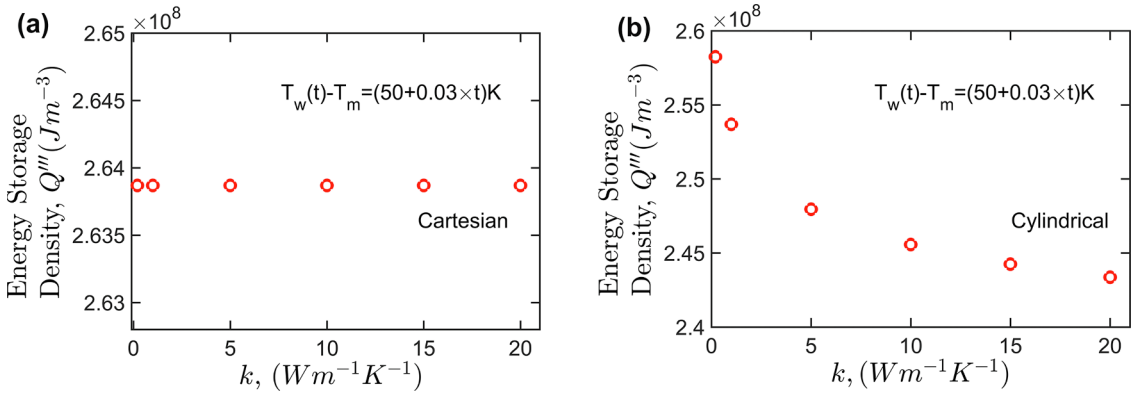

Fig. 9. Effect of thermal conductivity, k on energy storage density in (a) Cartesian and (b) Cylindrical coordinate systems for a time-dependent temperature boundary condition $T_w(t) - T_m = 50 + 0.03t$.

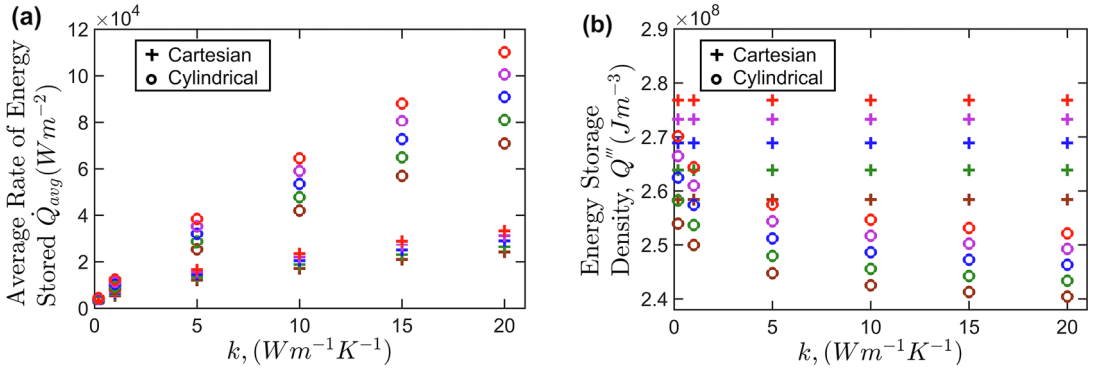

Fig. 10. Variation of (a) rate of energy storage and (b) energy storage density with thermal conductivity for various slopes B of linearly increasing temperature boundary condition, $T_w(t) - T_m = 50 + Bt$. Brown, green, blue, purple and red colors correspond to B = 0.01, 0.03, 0.05, 0.07 and 0.09 Ks^{-1} respectively. (For interpretation of the references to color in this figure legend, the reader is referred to the web version of this article.)

the energy storage density increases with increase in B. In contrast, energy storage density decreases with increasing k for the cylindrical system, which is consistent with previous results. The energy storage density increases with increasing B, which is explained by the greater impact on the rate of energy stored compared to phase change propagation, similar to the Cartesian result.

4. Conclusions

Understanding the impact of thermophysical properties on performance of phase change energy storage systems is very important for the design and optimization of several engineering systems. In the past, several papers have presented strategies for improving thermal conductivity of commonly used PCMs. The present work shows that while improving thermal conductivity is helpful for increasing the rate of energy stored, it is not similarly helpful for improving the energy storage density, which may be an important performance parameter in several applications. Using well-established theoretical models, the present work helps fully understand the impact of previously reported thermal conductivity enhancement on performance of phase change energy storage systems. Based on the theoretical model, the performance of various PCMs can be compared with each other, and the

optimal PCM can be chosen, depending of the relative importance of rate of energy stored and energy storage density, as well the geometry of energy storage system.

Acknowledgments

This material is based upon work supported by CAREER Award No. CBET-1554183 from the National Science Foundation.

Appendix 1. Equations for θ_2 and $\dot{Q}_{avg}$ in Section 2.2.2

An expression for θ_2 is given by

$$\theta_2 = \frac{f(t)}{128(\bar{y}(t))^4(\log\bar{y})^7}(40(f(t))^2\log\bar{y}(t) - 40(f(t))^2\log\bar{r} + 31(f(t))^2(\log\bar{y}(t))^2 + 10(f(t))^2(\log\bar{y}(t))^3 + 16(f^{'}(t))^2(\bar{y}(t))^2(\log\bar{y}(t))^3 + 29(f^{'}(t))^2$$
$$(\bar{y}(t))^2(\log\bar{y}(t))^4 + 14(f^{'}(t))^2(\bar{y}(t))^2(\log\bar{y}(t))^5 - 16(f^{'}(t))^2(\bar{y}(t))^4(\log\bar{y}(t))^3 + 8(f^{'}(t))^2(\bar{y}(t))^4(\log\bar{y}(t))^5 - 40(f(t))^2\log\bar{y}$$
$$(t)(\bar{r})^2 + 80(f(t))^2(\bar{y}(t))^2\log\bar{r} - 40(f(t))^2(\bar{y}(t))^4\log\bar{r} - 40(f(t))^2(\bar{y}(t))^2\log\bar{y}(t) - 31(f(t))^2\log\bar{y}$$
$$(t)\log\bar{r} - 40(f(t))^2(\bar{r})^2(\log\bar{y}(t))^2 - 16(f(t))^2(\bar{r})^2(\log\bar{y}(t))^3 + 9(f(t))^2(\bar{r})^4(\log\bar{y}(t))^2 + 6(f(t))^2(\bar{r})^4(\log\bar{y}(t))^3 + 40(f(t))^2(\bar{y}(t))^2(\log\bar{y}(t))^2 - 16$$
$$(f(t))^2(\bar{y}(t))^2(\log\bar{y}(t))^3 - 10(f(t))^2(\log\bar{y}(t))^2\log\bar{r} + 40(f(t))^2(\bar{y}(t))^2(\bar{r})^2\log\bar{y}(t) + 40(f(t))^2(\bar{r})^2\log\bar{y}(t)\log\bar{r} - 40(f(t))^2(\bar{y}(t))^2\log\bar{y}$$
$$(t)\log\bar{r} + 71(f(t))^2(\bar{y}(t))^4\log\bar{y}(t)\log\bar{r} - 56f(t)f^{'}(t)\bar{y}(t)(\log\bar{y}(t))^2 - 60f(t)f^{'}(t)\bar{y}(t)(\log\bar{y}(t))^3 - 19f(t)f^{'}(t)\bar{y}(t)(\log\bar{y}(t))^4 - 6f(t)f^{'}(t)$$
$$\bar{y}(t)(\log\bar{y}(t))^5 - 40(f(t))^2(\bar{y}(t))^2(\bar{r})^2(\log\bar{y}(t))^2 + 16(f(t))^2(\bar{y}(t))^2(\bar{r})^2(\log\bar{y}(t))^3 + 16(f(t))^2(\bar{r})^2(\log\bar{y}(t))^2\log\bar{r} - 6(f(t))^2(\bar{r})^4(\log\bar{y}(t))^2$$
$$\log\bar{r} - 4(f(t))^2(\bar{r})^4(\log\bar{y}(t))^3\log\bar{r} + 16(f(t))^2(\bar{y}(t))^2(\log\bar{y}(t))^2\log\bar{r} - 56(f(t))^2(\bar{y}(t))^4(\log\bar{y}(t))^2\log\bar{r} + 20(f(t))^2(\bar{y}(t))^4(\log\bar{y}(t))^3\log\bar{r} + 56f(t)$$
$$f^{'}(t)(\bar{y}(t))^3(\log\bar{y}(t))^2 - 40f(t)f^{'}(t)(\bar{y}(t))^3(\log\bar{y}(t))^3 + 16f(t)f^{'}(t)(\bar{y}(t))^3(\log\bar{y}(t))^5 + 8f(t)f^{''}(t)(\bar{y}(t))^2(\log\bar{y}(t))^3 + 13f(t)$$
$$f^{''}(t)(\bar{y}(t))^2(\log\bar{y}(t))^4 + 6f(t)f^{''}(t)(\bar{y}(t))^2(\log\bar{y}(t))^5 - 8f(t)f^{''}(t)(\bar{y}(t))^4(\log\bar{y}(t))^3 - 16(f^{'}(t))^2(\bar{y}(t))^2(\bar{r})^2(\log\bar{y}(t))^3 - 32(f^{'}(t))^2(\bar{y}(t))^2(\bar{r})^2$$
$$(\log\bar{y}(t))^4 - 16(f^{'}(t))^2(\bar{y}(t))^2(\bar{r})^2(\log\bar{y}(t))^5 + 16(f^{'}(t))^2(\bar{y}(t))^4(\bar{r})^2(\log\bar{y}(t))^3 + 3(f^{'}(t))^2(\bar{y}(t))^2(\bar{r})^4(\log\bar{y}(t))^4 - 8(f^{'}(t))^2(\bar{y}(t))^4(\bar{r})^2(\log\bar{y}(t))^5 + 2$$
$$(f^{'}(t))^2(\bar{y}(t))^2(\bar{r})^4(\log\bar{y}(t))^5 - 16(f^{'}(t))^2(\bar{y}(t))^2(\log\bar{y}(t))^2\log\bar{r} - 29(f^{'}(t))^2(\bar{y}(t))^2(\log\bar{y}(t))^3\log\bar{r} - 14(f^{'}(t))^2(\bar{y}(t))^2(\log\bar{y}(t))^4$$
$$\log\bar{r} + 32(f^{'}(t))^2(\bar{y}(t))^4(\log\bar{y}(t))^2\log\bar{r} + 16(f^{'}(t))^2(\bar{y}(t))^4(\log\bar{y}(t))^3\log\bar{r} - 8(f^{'}(t))^2(\bar{y}(t))^4(\log\bar{y}(t))^4\log\bar{r} - 16(f^{'}(t))^2(\bar{y}(t))^6(\log\bar{y}(t))^2$$
$$\log\bar{r} + 13(f^{'}(t))^2(\bar{y}(t))^6(\log\bar{y}(t))^3\log\bar{r} - 40(f(t))^2(\bar{y}(t))^2(\bar{r})^2(\log\bar{y}(t))^4\log\bar{r} + 56f(t)f^{'}(t)\bar{y}(t)(\bar{r})^2(\log\bar{y}(t))^2 + 72f(t)f^{'}(t)\bar{y}(t)(\bar{r})^2(\log\bar{y}(t))^3 + 24f(t)$$
$$f^{'}(t)\bar{y}(t)(\bar{r})^2(\log\bar{y}(t))^4 + 8f(t)f^{'}(t)\bar{y}(t)(\bar{r})^2(\log\bar{y}(t))^5 - 12f(t)f^{'}(t)\bar{y}(t)(\bar{r})^4(\log\bar{y}(t))^3 - 5f(t)f^{'}(t)\bar{y}(t)(\bar{r})^4(\log\bar{y}(t))^4 - 2f(t)f^{'}(t)$$
$$\bar{y}(t)(\bar{r})^4(\log\bar{y}(t))^5 - 60f(t)f^{'}(t)\bar{y}(t)(\log\bar{y}(t))^2\log\bar{r} + 19f(t)f^{'}(t)\bar{y}(t)(\log\bar{y}(t))^3\log\bar{r} - 112f(t)f^{'}(t)(\bar{y}(t))^3\log\bar{y}$$
$$(t)\log\bar{r} + 6f(t)f^{'}(t)\bar{y}(t)(\log\bar{y}(t))^4\log\bar{r} + 56f(t)f^{'}(t)(\bar{y}(t))^5\log\bar{y}(t)\log\bar{r} + 40(f(t))^2(\bar{y}(t))^2(\bar{r})^2(\log\bar{y}(t))^2\log\bar{r} - 16(f(t))^2(\bar{y}(t))^2(\bar{r})^2(\log\bar{y}(t))^3$$
$$\log\bar{r} - 56f(t)f^{'}(t)(\bar{y}(t))^3(\bar{r})^2(\log\bar{y}(t))^2 + 40f(t)f^{'}(t)(\bar{y}(t))^3(\bar{r})^2(\log\bar{y}(t))^3 - 16f(t)f^{'}(t)(\bar{y}(t))^3(\bar{r})^2(\log\bar{y}(t))^5 - 8f(t)f^{''}(t)(\bar{y}(t))^2(\bar{r})^2(\log\bar{y}(t))^3 - 16$$
$$f(t)f^{''}(t)(\bar{y}(t))^2(\bar{r})^2(\log\bar{y}(t))^4 - 8f(t)f^{''}(t)(\bar{y}(t))^2(\bar{r})^2(\log\bar{y}(t))^5 + 8f(t)f^{''}(t)(\bar{y}(t))^4(\bar{r})^2(\log\bar{y}(t))^3 + 3f(t)f^{''}(t)(\bar{y}(t))^2(\bar{r})^4(\log\bar{y}(t))^4 + 2f(t)$$
$$f^{''}(t)(\bar{y}(t))^2(\bar{r})^4(\log\bar{y}(t))^5 + 24f(t)f^{''}(t)(\bar{y}(t))^3(\log\bar{y}(t))^2\log\bar{r} + 8f(t)f^{'}(t)(\bar{y}(t))^3(\log\bar{y}(t))^3\log\bar{r} - 16f(t)f^{'}(t)(\bar{y}(t))^3(\log\bar{y}(t))^3$$
$$\log\bar{r} - 84f(t)f^{'}(t)(\bar{y}(t))^5(\log\bar{y}(t))^2\log\bar{r} + 45f(t)f^{'}(t)(\bar{y}(t))^5(\log\bar{y}(t))^3\log\bar{r} - 8f(t)f^{''}(t)(\bar{y}(t))^2(\log\bar{y}(t))^2\log\bar{r} - 13f(t)f^{''}(t)(\bar{y}(t))^2(\log\bar{y}(t))^3$$
$$\log\bar{r} - 6f(t)f^{''}(t)(\bar{y}(t))^2(\log\bar{y}(t))^4\log\bar{r} + 16f(t)f^{''}(t)(\bar{y}(t))^4(\log\bar{y}(t))^2\log\bar{r} + 8f(t)f^{''}(t)(\bar{y}(t))^4(\log\bar{y}(t))^3\log\bar{r} - 8f(t)f^{''}(t)(\bar{y}(t))^6(\log\bar{y}(t))^2$$
$$\log\bar{r} + 5f(t)f^{''}(t)(\bar{y}(t))^6(\log\bar{y}(t))^3\log\bar{r} + 56f(t)f^{'}(t)\bar{y}(t)\log\bar{y}(t)\log\bar{r} + 16(f^{'}(t))^2(\bar{y}(t))^2(\bar{r})^2(\log\bar{y}(t))^3\log\bar{r} + 16(f^{'}(t))^2(\bar{y}(t))^2(\bar{r})^2(\log\bar{y}(t))^4$$
$$\log\bar{r} - 16(f^{'}(t))^2(\bar{y}(t))^4(\bar{r})^2(\log\bar{y}(t))^3\log\bar{r} + 8(f^{'}(t))^2(\bar{y}(t))^4(\bar{r})^2(\log\bar{y}(t))^4\log\bar{r} - 2(f^{'}(t))^2(\bar{y}(t))^2(\bar{r})^4(\log\bar{y}(t))^4\log\bar{r} + 56(f^{'}(t))^2(\bar{y}(t))^3(\bar{r})^2(\log\bar{y}(t))^2$$
$$\log\bar{r} - 48f(t)f^{'}(t)(\bar{y}(t))^3(\bar{r})^2(\log\bar{y}(t))^3\log\bar{r} + 16f(t)f^{'}(t)(\bar{y}(t))^3(\bar{r})^2(\log\bar{y}(t))^4\log\bar{r} + 8f(t)f^{''}(t)(\bar{y}(t))^2(\bar{r})^2(\log\bar{y}(t))^3\log\bar{r} + 8f(t)$$
$$f^{''}(t)(\bar{y}(t))^2(\bar{r})^2(\log\bar{y}(t))^4\log\bar{r} - 8f(t)f^{''}(t)(\bar{y}(t))^4(\bar{r})^2(\log\bar{y}(t))^3\log\bar{r} - 2f(t)f^{''}(t)(\bar{y}(t))^4(\bar{r})^4(\log\bar{y}(t))^4\log\bar{r} - 56f(t)f^{'}(t)\bar{y}(t)(\bar{r})^2(\log\bar{y}(t))^2$$
$$\log\bar{r} - 32f(t)f^{'}(t)\bar{y}(t)(\bar{r})^2(\log\bar{y}(t))^3\log\bar{r} - 8f(t)f^{'}(t)\bar{y}(t)(\bar{r})^2(\log\bar{y}(t))^4\log\bar{r} + 8f(t)f^{'}(t)\bar{y}(t)(\bar{r})^4(\log\bar{y}(t))^3\log\bar{r} + 2f(t)f^{'}(t)\bar{y}(t)(\bar{r})^4(\log\bar{y}(t))^4\log\bar{r})q$$

An expression for $\dot{Q}_{avg}$ is given by

$$\dot{Q}_{avg}(t) = \frac{1}{t}\int_0^t -k(2\pi Rh)\left(\frac{dT}{dx}\right)_{x=R}d\tau$$
$$= \int_0^t -k(2\pi Rh)(T_w - T_m)\frac{1}{R}\left(-\frac{f(t)}{\log\bar{y}(t)} - \frac{(Ste)f(t)}{4(\bar{y}(t))^2(\log\bar{y}(t))^3}(f(t) - f(t)(\bar{y}(t))^2 + f(t)\log\bar{y}(t) - 2f^{'}(t)y(t)(\log\bar{y}(t))^2 - 2f^{'}(t)\bar{y}(t)(\log\bar{y}(t))^3 + f^{'}(t)(\bar{y}(t))^3\log\bar{y}\right.$$
$$(t) + f(t)(\bar{y}(t))^2\log\bar{y}(t) - f^{'}(t)y(t)\log\bar{y}(t)) - \frac{(Ste)^2f(t)}{128(\bar{y}(t))^4(\log\bar{y}(t))^7}(40(f(t))^2 - 80(f(t))^2(\bar{y}(t))^2 + 40(f(t))^2(\bar{y}(t))^4 + 71(f(t))^2\log\bar{y}(t) + 44(f(t))^2(\log\bar{y}(t))^2$$
$$+ 12(f(t))^2(\log\bar{y}(t))^3 + 16(f^{'}(t))^2(\bar{y}(t))^2(\log\bar{y}(t))^2 + 45(f^{'}(t))^2(\bar{y}(t))^2(\log\bar{y}(t))^3 + 52(f^{'}(t))^2(\bar{y}(t))^2(\log\bar{y}(t))^4 - 32(f^{'}(t))^2(\bar{y}(t))^4(\log\bar{y}(t))^2$$
$$+ 24(f^{'}(t))^2(\bar{y}(t))^2(\log\bar{y}(t))^5 - 32(f^{'}(t))^2(\bar{y}(t))^4(\log\bar{y}(t))^3 + 16(f^{'}(t))^2(\bar{y}(t))^6(\log\bar{y}(t))^2 + 16(f^{'}(t))^2(\bar{y}(t))^4(\log\bar{y}(t))^5 - 13(f^{'}(t))^2(\bar{y}(t))^6(\log\bar{y}(t))^3$$
$$- 71(f(t))^2(\bar{y}(t))^4\log\bar{y}(t) + 24(f(t))^2(\bar{y}(t))^2(\log\bar{y}(t))^2 - 16(f(t))^2(\bar{y}(t))^2(\log\bar{y}(t))^3 + 56(f(t))^2(\bar{y}(t))^4(\log\bar{y}(t))^2 - 20(f(t))^2(\bar{y}(t))^4(\log\bar{y}(t))^3$$
$$- 116f(t)f^{'}(t)\bar{y}(t)(\log\bar{y}(t))^2 - 91f(t)f^{'}(t)\bar{y}(t)(\log\bar{y}(t))^3 + 112f(t)f^{'}(t)(\bar{y}(t))^3\log\bar{y}(t) - 28f(t)f^{'}(t)\bar{y}(t)(\log\bar{y}(t))^4 - 8f(t)f^{'}(t)\bar{y}(t)(\log\bar{y}(t))^5$$
$$- 56f(t)f^{'}(t)(\bar{y}(t))^5\log\bar{y}(t) + 32f(t)f^{'}(t)(\bar{y}(t))^3(\log\bar{y}(t))^2 - 40f(t)f^{'}(t)(\bar{y}(t))^3(\log\bar{y}(t))^3 + 84f(t)f^{'}(t)(\bar{y}(t))^5(\log\bar{y}(t))^2 + 32f(t)f^{'}(t)(\bar{y}(t))^3(\log\bar{y}(t))^5$$
$$- 45f(t)f^{'}(t)(\bar{y}(t))^5(\log\bar{y}(t))^3 + 8f(t)f^{''}(t)(\bar{y}(t))^2(\log\bar{y}(t))^2 + 21f(t)f^{''}(t)(\bar{y}(t))^2(\log\bar{y}(t))^3 + 20f(t)f^{''}(t)(\bar{y}(t))^2(\log\bar{y}(t))^4 - 16f(t)f^{''}(t)(\bar{y}(t))^4(\log\bar{y}(t))^2$$
$$\left.+ 8f(t)f^{''}(t)(\bar{y}(t))^2(\log\bar{y}(t))^5 - 16f(t)f^{''}(t)(\bar{y}(t))^4(\log\bar{y}(t))^3 + 8f(t)f^{''}(t)(\bar{y}(t))^6(\log\bar{y}(t))^2 - 5f(t)f^{''}(t)(\bar{y}(t))^6(\log\bar{y}(t))^3 - 56f(t)f^{'}(t)\log\bar{y}(t))\right)d\tau$$

References

[1] Z. Ling, Z. Zhang, G. Shi, X. Fang, L. Wang, X. Gao, et al., Review on thermal management systems using phase change materials for electronic components, Li-ion batteries and photovoltaic modules, Renew. Sustain. Energy Rev. 31 (2014) 427–438, https://doi.org/10.1016/j.rser.2013.12.017.

[2] A. Sharma, V. Tyagi, C. Chen, D. Buddhi, Review on thermal energy storage with phase change materials and applications, Renew. Sustain. Energy Rev. 13 (2009) 318–345, https://doi.org/10.1016/j.rser.2007.10.005.

[3] M.M. Farid, A.M. Khudhair, S.A.K. Razack, S. Al-Hallaj, A review on phase change energy storage: materials and applications, Energy Convers. Manage. 45 (2004) 1597–1615, https://doi.org/10.1016/j.enconman.2003.09.015.

[4] S. Hasnain, Review on sustainable thermal energy storage technologies, Part I: heat storage materials and techniques, Energy Convers. Manage. 39 (1998) 1127–1138, https://doi.org/10.1016/s0196-8904(98)00025-9.

[5] J. Cot-Gores, A. Castell, L.F. Cabeza, Thermochemical energy storage and conversion: A-state-of-the-art review of the experimental research under practical conditions, Renew. Sustain. Energy Rev. 16 (2012) 5207–5224, https://doi.org/10.1016/j.rser.2012.04.007.

[6] K. Shah, N. Balsara, S. Banerjee, et al., State-of-the-art and future research needs for multiscale analysis of Li-ion cells, ASME J. Electrochem. Energy Convers. Storage 14 (020801) (2017) 1–17, https://doi.org/10.1115/1.4036456.

[7] L. Fan, J. Khodadadi, Thermal conductivity enhancement of phase change materials for thermal energy storage: a review, Renew. Sustain. Energy Rev. 15 (2011) 24–46, https://doi.org/10.1016/j.rser.2010.08.007.

[8] A. Mostafavi, M. Parhizi, A. Jain, Theoretical modeling and optimization of fin-based enhancement of heat transfer into a phase change material, Int. J. Heat Mass Transf. (2019) (in review).

[9] L. Liu, D. Su, Y. Tang, G. Fang, Thermal conductivity enhancement of phase change materials for thermal energy storage: a review, Renew. Sustain. Energy Rev. 62 (2016) 305–317, https://doi.org/10.1016/j.rser.2016.04.057.

[10] B. Zalba, Marín José Ma, L.F. Cabeza, H. Mehling, Review on thermal energy storage with phase change: materials, heat transfer analysis and applications, Appl. Therm. Eng. 23 (2003) 251–283, https://doi.org/10.1016/s1359-4311(02)00192-8.

[11] F. Agyenim, N. Hewitt, P. Eames, M. Smyth, A review of materials, heat transfer and phase change problem formulation for latent heat thermal energy storage systems (LHTESS), Renew. Sustain. Energy Rev. 14 (2010) 615–628, https://doi.org/10.1016/j.rser.2009.10.015.

[12] T. Oya, T. Nomura, M. Tsubota, N. Okinaka, T. Akiyama, Thermal conductivity enhancement of erythritol as PCM by using graphite and nickel particles, Appl. Therm. Eng. 61 (2013) 825–828, https://doi.org/10.1016/j.applthermaleng.2012.05.033.

[13] J. Fukai, M. Kanou, Y. Kodama, O. Miyatake, Thermal conductivity enhancement of energy storage media using carbon fibers, Energy Convers. Manage. 41 (2000) 1543–1556, https://doi.org/10.1016/s0196-8904(99)00166-1.

[14] A. Karaipekli, A. Sarı, K. Kaygusuz, Thermal conductivity improvement of stearic acid using expanded graphite and carbon fiber for energy storage applications, Renew. Energy 32 (2007) 2201–2210, https://doi.org/10.1016/j.renene.2006.11.011.

[15] A. Mills, M. Farid, J. Selman, S. Al-Hallaj, Thermal conductivity enhancement of phase change materials using a graphite matrix, Appl. Therm. Eng. 26 (2006) 1652–1661, https://doi.org/10.1016/j.applthermaleng.2005.11.022.

[16] A. Sarı, A. Karaipekli, Preparation, thermal properties and thermal reliability of palmitic acid/expanded graphite composite as form-stable PCM for thermal energy storage, Sol. Energy Mater. Sol. Cells 93 (2009) 571–576, https://doi.org/10.1016/j.solmat.2008.11.057.

[17] P. Keblinski, S. Phillpot, S. Choi, J. Eastman, Mechanisms of heat flow in suspensions of nano-sized particles (nanofluids), Int. J. Heat Mass Transf. 45 (2002) 855–863, https://doi.org/10.1016/s0017-9310(01)00175-2.

[18] D.W. Hahn, M.N. Özişik, Heat Conduction, third ed., John Wiley & Sons, Hoboken, New Jersey, 2012.

[19] J. Stefan, Ueber die Theorie der Eisbildung, insbesondere über die Eisbildung im Polarmeere, Ann. Phys. 278 (1891) 269–286, https://doi.org/10.1002/andp.18912780206.

[20] J. Caldwell, Y. Kwan, On the perturbation method for the Stefan problem with time-dependent boundary conditions, Int. J. Heat Mass Transf. 46 (2003) 1497–1501, https://doi.org/10.1016/s0017-9310(02)00415-5.

[21] G. Lock, J. Gunderson, D. Quon, J. Donnelly, A study of one-dimensional ice formation with particular reference to periodic growth and decay, Int. J. Heat Mass Transf. 12 (1969) 1343–1352, https://doi.org/10.1016/0017-9310(69)90021-0.